DESIGN AND OPTIMIZATION OF A TOMOSYNTHESIS SYSTEM USING A MULTIPLE X-RAY SOURCE BASED ON CARBON NANOTUBES

A.Frassati[(1)], V.Rebuffel[(2)], V.Moulin[(2)]
[(1)]INSA-CNDRI, Bat St-Exupery, 25 av. J.Capelle, 69621 Villeurbanne Cedex, France
[(2)]CEA-LETI, 17 rue des Martyrs, 38054 Grenoble Cedex 9, France

Abstract

Through a French collaborative project, we are developing a new concept of portable X-ray system for the inspection of abandoned luggage. Innovation relies on the use of a multiple X-Ray source, based on a new beam type composed of carbon nanotubes photo-cathodes controlled by laser diode, allowing numerous emission spots without mechanical motion. This paper presents the design of the geometry of a tomosynthesis system using this source, aiming at providing 3D information on the examined object. Several figures of merit estimated on the volume, characterizing image quality, noise, and time, are proposed and used to optimize the system. A dedicated reconstruction algorithm, based on an iterative technique implemented within a multi-resolution approach has been developed. First evaluations are performed on simulated radiographs.

Key words: X-ray, tomosynthesis, tomography, reconstruction, multi-resolution, multi-source.

1. Introduction

In conventional tomography, a plane of interest is produced by rotating the detector and the X-ray tube around the inspected object, or equivalently by rotating the object in a detector-tube system. Unfortunately, such acquisition geometry is not allowed in some configurations. In this case, tomosynthesis – sometimes called planar tomogaphy – is an alternative technique able to provide 3D information about the examined object. The X-ray tube is generally moved along a trajectory within a plane that is parallel to the detector plane. The sequence of acquired radiographs is combined by an algorithm to provide reconstructed planes parallel to the detector one. Despite the poor depth resolution inherent to the system geometry, tomosynthesis is an X-ray technique that is increasingly used in both NDT and security applications.

We consider the case of the inspection of an abandoned luggage. The objective is the detection of illicit materials – explosive or chemical hazards - in the luggage, using a portable, fast, and reliable system. The constraints differ from security airport systems. Today, the inspection is performed by radiography. A thin detector is carefully placed behind the luggage, the tube on the ground, and a radiograph along the horizontal axis is acquired. If the luggage is large, a second radiograph may eventually be acquired after a manual shift of the detector. Standard tomography technique is not possible due to the lack of place around the luggage, which may be located close to a wall – moreover, mechanical motion close to unknown content and potentially dangerous luggage should be avoided. Displacement of the luggage itself is obviously forbidden. Tomosynthesis is a particularly convenient technique for this configuration.

Through a French collaborative project, we are developing a new concept of portable X-ray system for the inspection of abandoned luggage. One innovative aspect relies on the combined use of two complementary imaging X-ray techniques, transmission and diffraction. In the present paper we detail the system functionality based on transmission X-ray technique. The other functionality, which is the material characterization using a diffraction technique, is presented in [1].

Our system benefits from new technological developments in the domain of X-ray emission devices. We investigate the use of a multiple X-Ray source with several emission spots distributed

over a large area. This source, under development at Thales, is based on a new beam type composed of carbon nanotubes photo-cathodes controlled by laser diode [2]. The emission properties of the carbon nanotubes have been characterized. The multi-source design takes into account the portability constraint, insisting on compacity and integration of high voltage power. The major difference with a conventional X-ray tube is the possibility to switch between the source spots almost instantaneously and without mechanical motion – allowing a tomosynthesis system particularly convenient in the case of a suspicious abandoned luggage.
The present paper focuses on two aspects: system design (§2), and dedicated algorithm development (§3). The different source spots are distributed in a plane parallel to the detector (figure 1). For a given sources configuration, a reconstructed volume can be obtained thanks to a standard tomosynthesis algorithm. We propose to evaluate several figures of merit on the volume, in order to optimize the system configuration in terms of number and location of sources. Then, for the chosen configuration, a dedicated algorithm is presented in §3. Based on an iterative reconstruction technique, the proposed algorithm is implemented within a multi-resolution approach.
All these studies are done with the help of the Sindbad simulation tool developed in our laboratory [3]. This software tool allows the description in a friendly interface of the detector, the source, and the object in terms of geometry and materials. Then realistic radiographs including noise and phenomenon such as scattering radiation can be provided in any acquisition geometry, and used for evaluation.

2. Tomosynthesis system design

2.1 System constraints and characteristics

To design and optimize the system geometry, we first list the constraints linked to the application context and system manufacturing. The detector used is a flat panel one or similar, and will remain static during the inspection. The various sources (or emission spots) are supposed to be included into a plane, called *sources plane*. The maximum size of this plane is 500×500mm², and the minimum distance between two sources is a few centimeters. The detector-source distance is varying between 500 and 1000mm. The parameters to be optimized are essentially the number of sources and their location within the sources plane. Figure 1 illustrates the system geometry (left) with a particular geometry (a configuration of sources called *network*), and (right) two other possible configurations, the *cross* and the *circle* ones.

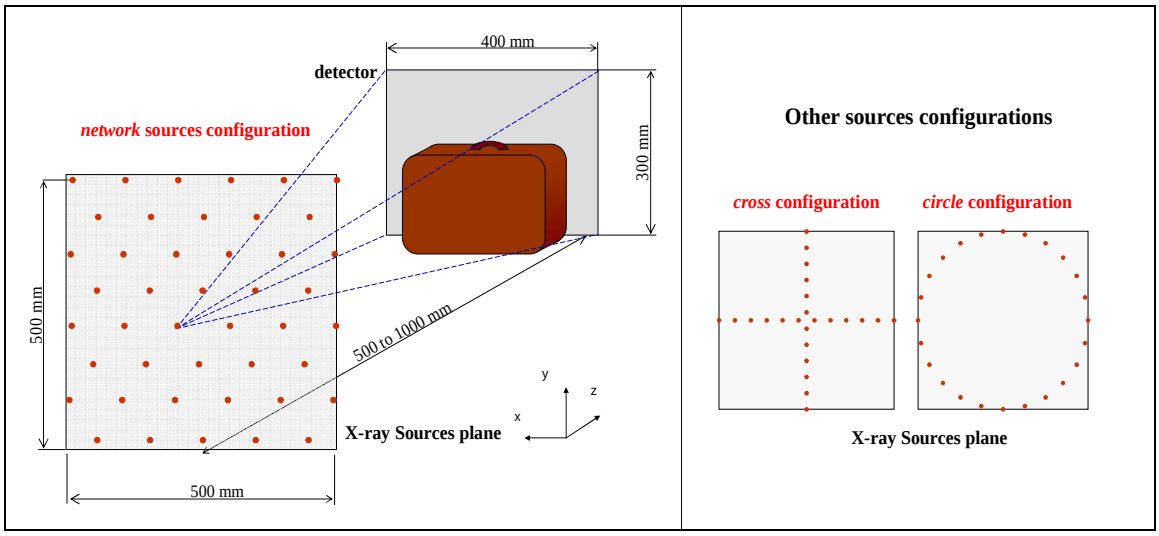

Figure 1: Geometry of our tomosynthesis system, and various possible sources configurations.

2.2 Evaluation criteria

The quality criterion should be evaluated on the reconstructed volume, and thus depends on the chosen reconstruction algorithm. From initial works in 1970's, many algorithms have been proposed, to combine the various radiographs acquired in tomosynthesis geometry. Mathematically, standard CT reconstruction can not be applied, and the alternative algorithms take into account more or less explicitly the bad conditioning of the problem inherent to the unconstrained geometry. A review can be found in [4]. We have implemented two algorithms: the conventional and fast shift-and-add algorithm, and an iterative method, the SART (Simultaneous Algebraic Reconstruction Technique [5]). Our version considers one block per radiograph, and the stopping criterion is the iterations number. For this phase of the study we do not need a more sophisticated algorithm, our purpose being the relative comparison of different system configurations. More precisely, we assume that improving the algorithm would not change the optimal configuration of sources, but only the absolute performance level.

Our evaluation approach is the following: we simulate a small attenuating ball included in a uniform luggage, at a given location. Using Sindbad software, we then simulate the sequence of radiographs corresponding to a given configuration of sources, on which we apply the reconstruction algorithm. Simulations are performed with and without photonic noise. On the obtained volume, we evaluate several criteria used as figures of merit, and quantifying noise, global time, and more importantly here, spatial resolution. Noise is estimated thanks to local variance, time includes acquisition and processing time. Spatial resolution in the plane parallel to detector is similar to those of radiographs, and spatial resolution along the source-detector axis, called *depth resolution*, is much poorer and characteristic of the system geometry. We estimate this resolution by the (normalized) difference between the grey level at ball position (z) and the level at a distance h, typically three times the ball diameter (figure 2, top right, shows these two planes):

$$C_{res}(h) = \frac{\max(z) - \max(z+h)}{\max(z)} \qquad \text{where typically } h = 3\phi.$$

Other possibilities would have been to consider the mean instead the max of values, or to compute the standard FWHM (full width at half maximum) of a profile along z-axis. This last one has been tested but as shown in Figure 2, the impulse response of tomosynthesis is spreading also in x-y out of focus planes. Furthermore the signal is not homogeneous in these planes and presents frequencies inducing artifacts, especially in case of low number of sources. The proposed criterion allows taking into account these artifacts induced in the out of focus planes. It has to be estimated on noise-free volumes, easily obtained by simulation. Our criterion ranges from 0 (no localization of the ball) to 1 (perfect localization). The ball size has been adapted to the minimum size of the structures to be detected. Finally, it is important to notice that the criterion may be not uniform inside the volume, and should be evaluated at different locations.

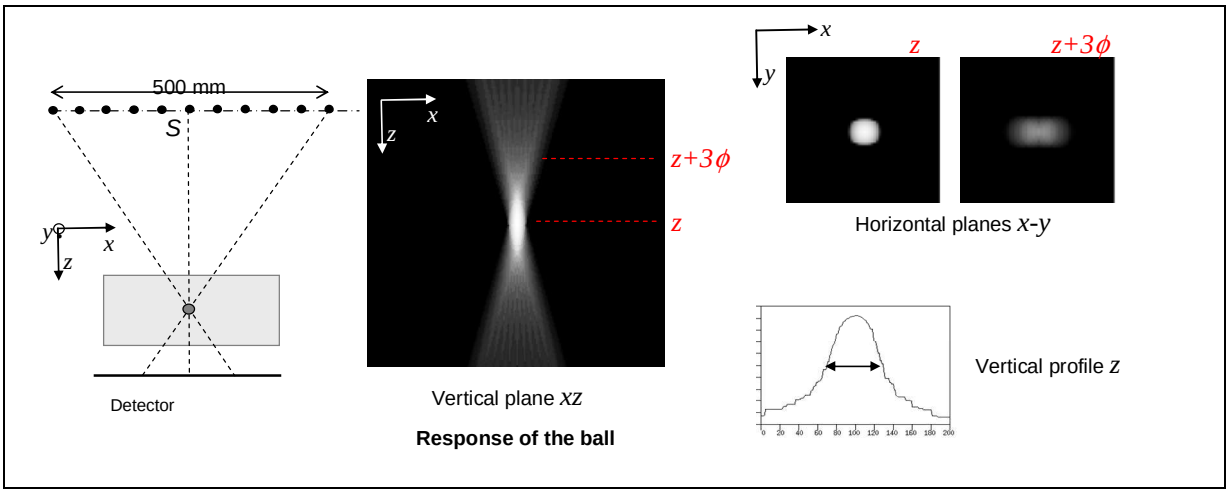

Figure 2: Reconstruction data volume used for the evaluation of depth resolution criterion.

2.3 Results of the system optimization in terms of sources configurations

First, the sources number is fixed and the different sources configurations are compared using the resolution criterion as figure of merit – the acquisition and processing times and the noise level being approximately constant. We particularly analyzed the *cross* and *circle* configurations, which are the more common ones in standard tomosynthesis with a mechanical source motion, and the *network* one, for which the sources are uniformly distributed within the plane (figure 1).
The *cross* configuration is the worse one, with a criterion C_{res}=0.75 at the center of the volume for a number of sources equal to 24. The *circle* and *network* configurations are better (about 0.9 for both), the *network* being clearly the best in terms of homogeneity, with a variation between the center and the corner of the volume smaller than 1%.
For practical reasons, other configurations achievable with a linear array of carbon nanotubes cathodes have been analyzed: linear array in translation (fig 3a), in rotation (3b) and rotation with irregularly distributed sources (3c). The a) configuration presents good performance (C_{res}=0.87 for 36 sources), similar to the *network* previously presented, the b) is significantly lower (0.65) but the c) is not so far from the a) configuration (0.82). In case of such a linear array of carbon nanotubes, the choice between a) or c) configuration would depend on other considerations such as the interest of presenting a static point for power cable.

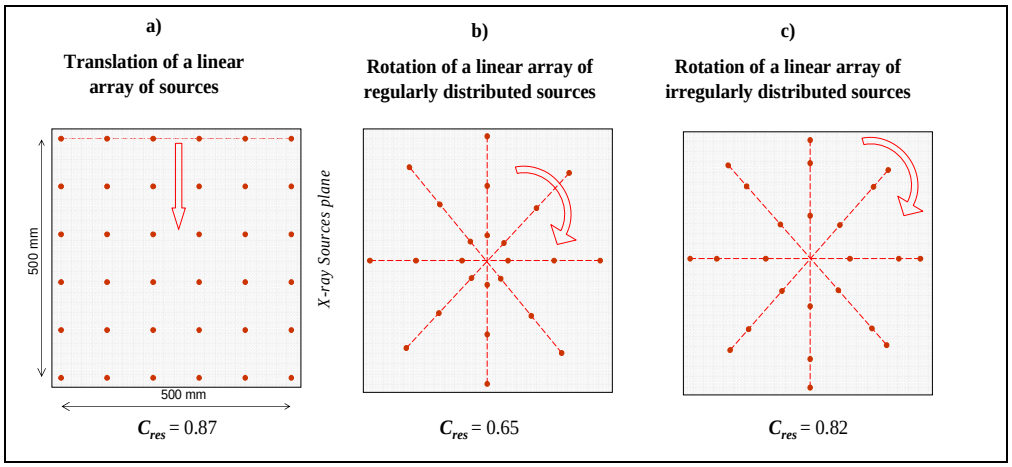

Figure 3: Sources configurations reachable with a linear array of carbon nanotubes.

2.4 Results of the system optimization in terms of sources number

The number of sources results from the compromise between reconstruction quality, noise level, acquisition and processing time. It has been optimized in the best configurations – *network* (figure 1, left) and linear array of sources in translation (figure 3a) which are closed together.

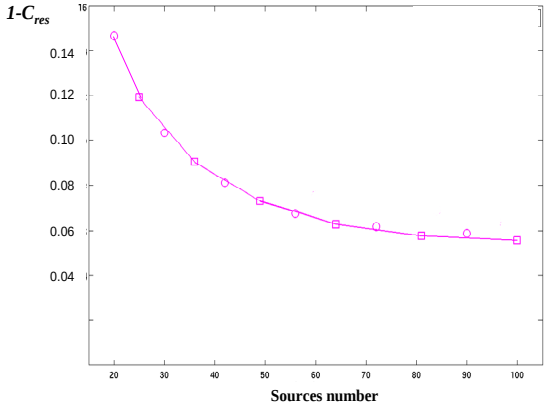

Figure 4: Depth resolution values (in fact, 1- C_{res}) function of sources number.

For image quality evaluation, we use the previous criterion C_{res} measuring depth resolution. Obtained values (in fact, of (1- C_{res})) are drawn in figure 4 for a number of sources varying between 20 and 100, and for a location at the center of the volume. As expected, the criterion increases with the source number. It does rapidly from 10 to 50 sources, slowly afterwards.

Noise level estimated on the reconstructed volume is another quantifier of image quality. We analyzed its dependency on the sources number, given a fixed total acquisition time (acquisition using all sources).
Let us consider photonic noise only; noise on one (attenuation) radiograph is linked to its acquisition time: $\sigma_{radio}^{\ 2} = \alpha / T_{radio}$. It has been demonstrated in case of tomographic reconstruction that noise on the reconstructed volume is given by: $\sigma_{vol}^{\ 2} = \frac{K}{T_{radio} \cdot N_{radio}}$ and depends only of the global acquisition time (K is a factor depending on algorithm, apodization filtering, resolution). In case of tomosynthesis, it is clear that for the simple shift-and-add algorithm, the formulae remains valid. We have checked using simulation that the formulae can be applied in case of SART algorithm – though noise level increases with SART iterations. In other words, for a given algorithm, the noise level will be similar for $N_{sources}$ of T_{radio} acquisition time each, or kN_{source}, with T_{radio}/k time each.
Nevertheless, this computation does not take into account the system aspect, and in fact the mechanical motion time T_{motion} may be not negligible. For conventional tomosynthesis, it occurs for each source location, inducing a global $N_{sources}T_{motion}$ non usable time. Using carbon nanotubes, the switch from one source to another one can be considered instantaneous thus T_{motion} can be neglected. For the solution using a linear array of carbon nanotubes cathodes, this time occurs for each position of the source array, the corresponding lost time is approximately $\sqrt{N_{sources}}T_{motion}$. The time available for acquisition ($T_{radio} \cdot N_{radio}$) is the difference between global time and motion time. As a consequence, the sources number has a strong influence on noise level in case of standard tomosynthesis, a slight one for a linear array of nanotubes sources, and no influence for a complete nanotubes sources system. Considering now the processing time, the implemented algorithm makes it be proportional to the sources number.
For the considered geometry, the compromise between quality criteria, noise and processing time leads to ~36-49 sources, as long as the corresponding time is acceptable. Furthermore, acceleration methods can be used, as detailed hereafter. The performance of the optimized system is as follows: depth resolution – estimated from the FWHM of the profile crossing a 1mm reconstructed structure – is about around 3.5mm in case of shift-and-add algorithm, and between 2 and 2.5mm for the SART one. Noise level is determined by the photons flux emitted by the source.

3. Dedicated reconstruction algorithm development

3.1 Reconstruction volume

The inspected luggage may clearly be larger than the detector, so than the field of view. Let us distinguish the totally imaged part of the object, and the partially imaged one (concerned by at least one projection), figure 5. The partially imaged part induces artifacts in the reconstruction volume, which can be enhanced by the iterative behavior of the algorithm. To get around the problem of these truncature artifacts, the usual way is to reconstruct only the totally imaged part, and/or develop corrected normalization weighting and extrapolation methods assuming that the partially imaged part is uniform (for instance [6] for breast tomosynthesis). In our context, the assumption of a uniform partially imaged part is not convenient, and furthermore, the structure of interest to be detected can be located in the partially imaged part. Consequently the volume of reconstruction is chosen equal to the partially imaged part (for practical reasons, to the parallelepiped just containing

it). The resulting processing time is important, but it will be reduced thanks to the multi-resolution method presented hereafter.

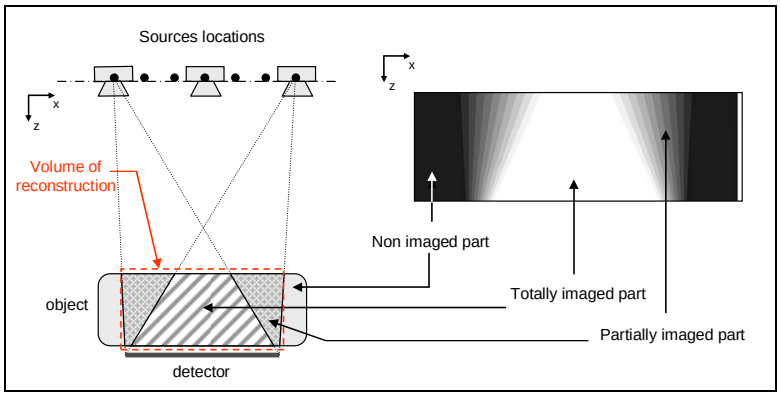

Figure 5: Partially and totally imaged part of the reconstruction volume.

3.2 Sampling of the reconstruction volume

Accordingly to the accuracy required in the final volume, detectors pixels should be about 0.5 mm sized – typically binned by factor 4 in case of a Thales flat panel. The spatial sampling of the reconstruction volume is fixed to 0.8 mm in the planes parallel to the detector. To take into account the poor depth resolution inherent to tomosynthesis geometry, and aiming at reducing data to be processed, we have tested various voxels sizes along depth axis: 0.8, 1.6, 3.2 and 6.4 mm. From 0.8 mm to 3.2 mm, a quality parameter quantifying resolution has been degraded by less than 5%, but has shown to decrease significantly from 6.4 mm, which is coherent with the depth resolution estimated previously. Consequently, the voxel size in depth axis will be fixed at 3.2 mm. This allows to reduce the amount of voxels of the reconstruction volume from 10^8 voxels (400×400×300 mm3 with a detector 400×400 and a luggage 300mm thick and 400mm large, voxels size 0.8mm3) to 2. 10^7 voxels.

3.3 Radiographs selection intervening in the SART algorithm

In the SART algorithm, blocks of data are successively taken into account to update the current state of volume under reconstruction. More precisely, one iteration step consists in the successive projection of each block, the computation of the error identified as the difference between current projection and true projection, and the weighted back projection of this error. Commonly, blocks are identified with radiographs. We tested different update orders of these blocks, and found the best one being a random order. Among the fact that a constant order favors the last considered radiograph, which may be dangerous in case of unexpected disturbances in this particular one, we noticed that a random order increases the convergence speed. On the simulated configurations, the level of convergence was similar for 6 iterations using a fixed scanning order, and 3 iterations in a random order. The level of convergence was the same for both after 10 iterations.
With the objective of accelerating the algorithm, we have also tested a modification of the blocks, where the first iteration considers only a subset of the blocks. For instance, in case of a 49 sources system, the gain between a SART algorithm (2 iterations), involving 49 sources, and a modified SART, composed of 1 iteration using 28 sources, followed by a second one using all the sources, is about 70% in time for a comparable image quality.

3.4 Multi-resolution approach

The main modification to the standard SART algorithm that we have developed is a multi-resolution approach to speed up the reconstruction process; the idea is to perform a coarse initialization of the reconstruction, then successive iterations from the coarsest scale to the finest one. Multi-resolution techniques are commonly used in tomography. For instance in [7], the

authors, within a Bayesian framework, apply a multi-resolution minimization function, allowing both a decrease of data to process and a better conditioned problem. Wavelets are frequently used in a multi-resolution approach ([8]). In tomosynthesis, multi-resolution approaches have been tested, generally associated to the MAP (a posteriori maximum) criterion [9].

We adapted the SART algorithm as follows: the radiograph are binned to be transformed at scale 1 (merging of 4 pixels) and scale 2 (merging of 16 pixels), scale 0 being the finest one; the initialization step is performed at scale 2 by shift-and-add computation, then *k* iterations of SART are performed at scale 2, then *k* at scale 1, and finally *k* at scale 0. The *k* parameter is the number of iterations per scale. Scales coarser than 2 have also been tested. The transform of the volume from one scale to the finer one, requiring a sub-sampling of 1 voxel to 8 voxels, is implemented using an interpolation that has been proved to be necessary.

To evaluate the proposed algorithm, we have simulated a test object composed of two small Aluminum balls, diameter 6 and 10mm, distant by 20mm along the depth direction. These balls are included in a Plexiglas background. The reconstruction volume here is $120^3 mm^3$. A figure of merit is defined as the ratio max / min of a depth profile crossing the balls (Figure 6). If the balls are not separable at all, this ratio is equal to 1, and increases with separability. Evaluations have been done at standard depth sampling (0.8mm) and adapted sampling (3.2mm, as explained in §3.2). Software code is not optimized, and is running on a bi-processor 2.6 GHz workstation. For the considered volume 200^3 voxels, processing time for one iteration is 4mn40 at scale 0, 22s at scale 1, and 1s at scale 2. Results using various versions of the algorithm are presented in Figure 7.

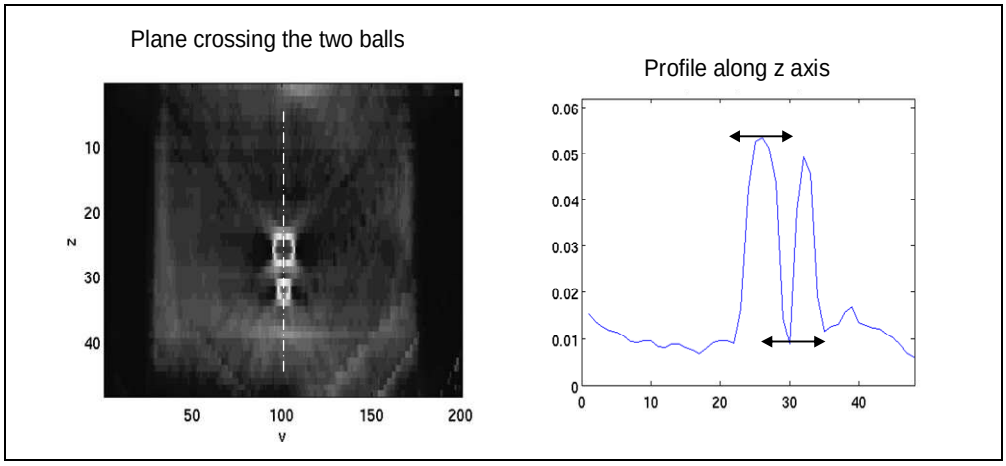

Figure 6: Reconstruction of two superimposed small balls, 1 iteration per scale, from scale 2 to 0.

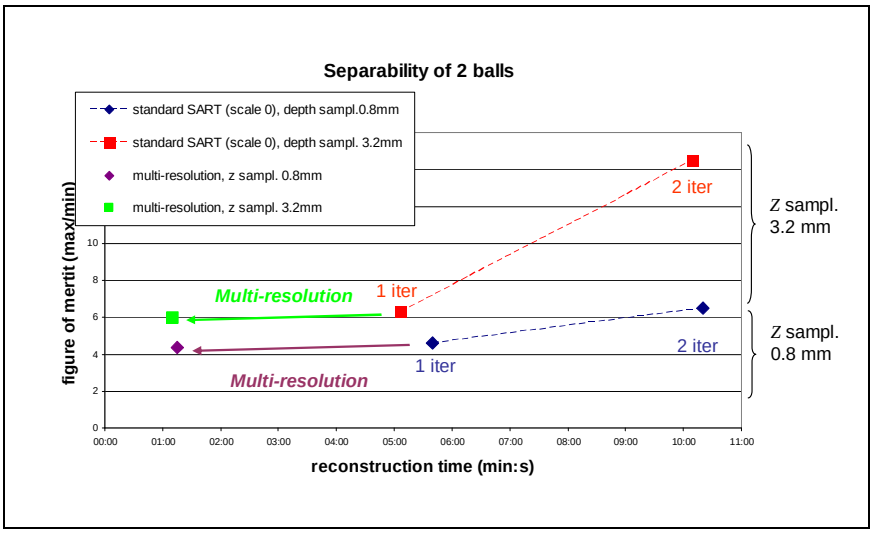

Figure 7: Performance (image quality versus time) for different versions of the algorithm.

On figure 7, blue dots correspond to different numbers of iterations of standard SART algorithm at initial depth sampling (0.8mm). With increasing iterations, image quality in terms of separability of objects of interest improves, but processing time increases (only 1 and 2 iterations are drawn for visibility purpose). This trend is the same for all the algorithm versions. In case of optimized depth sampling (3.2 mm, discussed at §3.2), we get the red curve. When applying the multiresolution approach with coarser scale being 2 (initialization at scale 2, then 1 iteration at scale 1, and finally 1 iteration at scale 0), we get the violin dot for depth sampling 0.8mm – to be compared with blue curve) and green dot for depth sampling 3.2 mm – to be compared with red curve.
To conclude this study, the implemented multi-resolution approach allows a gain in time of a factor about five, with a comparable reconstruction quality in terms of depth resolution. Similar simulations have been performed including photonic noise, without significant modification of the behavior of the multi-resolution version of the algorithm. Of course, the applied SART algorithm being not regularized, noise level increases with iterations – independently of any multi-resolution scheme.

4. Representative examples

Using the proposed tomosynthesis algorithm, implemented in a multi-resolution framework, we have computed the reconstructed volumes from simulated radiographs of representative objects.
Figure 8 illustrates the case of a detonator hidden inside a pen. Four felt pens are included inside a luggage, with a local uniform background. Such pens commonly contain a steel spring, strongly attenuating for X-ray, which appears in white on tomosynthesis planes corresponding to pens 1, 2 and 4. In the third pen, the spring has been changed for a detonator, which is clearly visible on the corresponding plane, though all structures were superimposed on the radiograph. Artifacts visible in the reconstructed planes are due to the high attenuation of the steel springs.

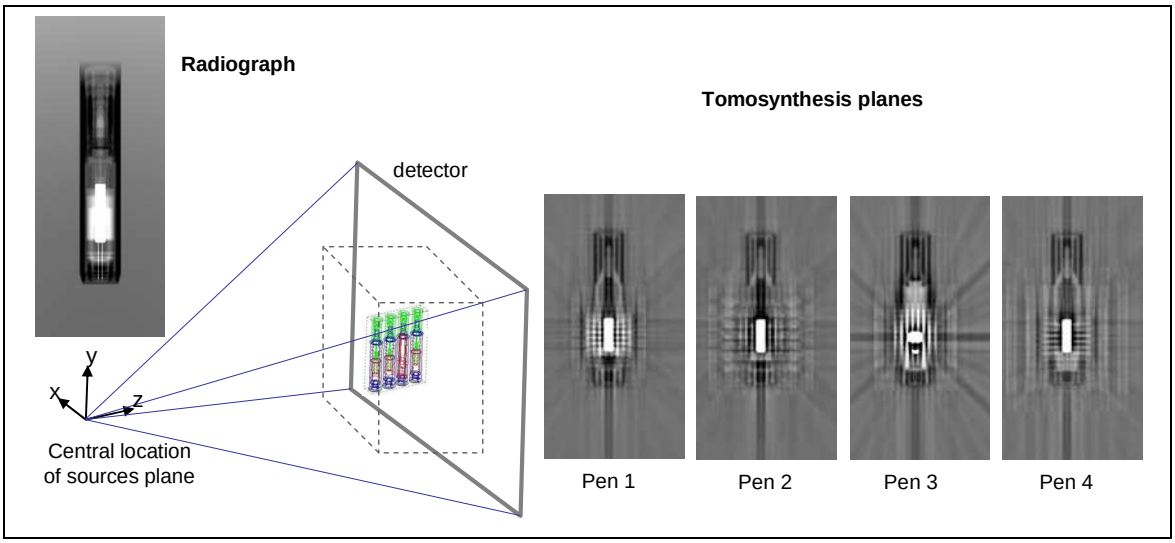

Figure 8: Example of tomosynthesis reconstruction of four superimposed felt pens. The third one contains a detonator replacing its spring, visible on tomosynthesis plane only.

Another simulated example is shown in figure 9. Four felt batteries are included inside a luggage. One battery contains a detonator, perfectly visible on the tomosynthesis plane, much better than on the radiograph. For this example, results are shown both with a standard version of SART, using 0.8mm depth sampling, and for a multi-resolution version, using 3.2mm depth sampling. Results are comparable, though processing time has been divided by 6.

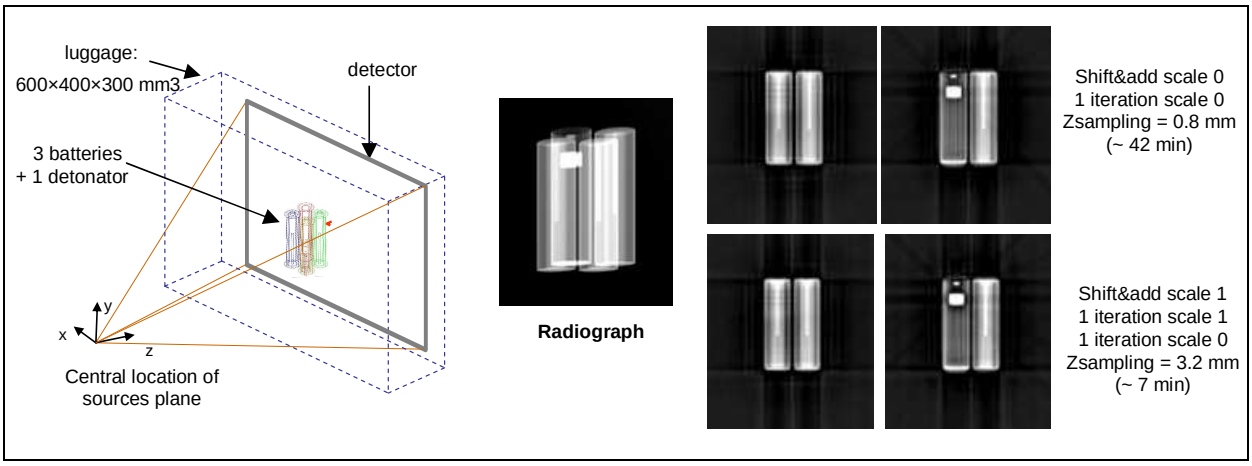

Figure 9: Example of tomosynthesis reconstruction of four batteries, one of them containing a detonator. Results can be compared between the standard version of the algorithm and the proposed one.

5. Discussion and conclusion

We have designed a tomosynthesis geometry for a portable system dedicated to the inspection of suspicious abandoned luggage. An important specificity of this system is the use of a multiple X-Ray source with several emission spots distributed over a large area. This source is based on a new beam type composed of carbon nanotubes photo-cathodes controlled by laser diode. The major difference with a conventional X-ray tube is the possibility to switch between the source spots almost instantaneously and without mechanical motion. The challenge was to optimize the distribution and number of sources locations. We developed a depth resolution figure of merit, integrating artifact quantification. Compromise was found between image quality, noise level and reconstruction time. Finally we proposed an optimal system configuration, based on 36-49 sources regularly distributed in the source plane.

For this optimal configuration, the reconstruction algorithm has been optimized, essentially by implementing a multi-resolution framework to speed up the processing time. We adapted an iterative SART algorithm in the following way: an initialization step is performed a rough scale by shift-and-add algorithm using binned radiographs, then successive steps corresponding to progressively finer resolution scales are applied, k iterations being processed per scale. The k parameter is tuned depending on the acceptable noise level defined by the end-user. For the studied examples, we used three scale levels, and performed 1 or 2 iterations per scale. The gain in time reached by this approach (around 5) allows us to consider the maximal reconstruction volume, which is required for our application context. For a representative volume sized 450×450×300mm, sampling steps 0.8mm in planes parallel to detector, and 3.2 mm along depth axis, the current processing time is about 7mn. To conclude, the developed algorithm provides a sufficiently fine result after some minutes for typical volume size; furthermore, the initial coarse result is available very quickly to start the human inspection process while waiting the fine result.

An experimental prototype should be available in mid-2010, and will be used to confirm experimentally our conclusions. It is important to notice that such multi-sources systems, associated to adapted algorithm, could benefit to many other applications, for instance high speed tomography for 3D imagery of transitory phenomenon, or more generally should allow new 3D geometry for tomography.

Acknowledgment

This work has been partially funded by French collaborative project ANR CSOSG 2007 n°14 SPIDERS. The authors would like to thank the other partners for their help, especially in providing information on the other components of the system.

References

[1] P. Ponard & al., "Etude des géométries d'acquisition en tomosynthèse et diffraction associées à une multi-sources RX à nanotubes de carbone photo-contrôlés", proc. of Workshop on global security (WISG - 2010), Troyes (France), january 2010 – *in French*.

[2] L. Hudanski, E. Minoux, L. Gangloff, K.B.K. Teo, J.-P. Schnell, S. Xavier, W.I. Milne, D. Pribat, J. Robertson, P. Legagneux, "Carbon nanotube based photocathode", Nanotechnology 19 105201 (2008).

[3] J.Tabary, P.Hugonnard, F.Mathy, "SINDBAD: a realistic multi-purpose and scalable X-ray simulation tool for NDT application", Proc. of DIR2007, Lyon, june 2007.

[4] J.Dobbins, D.Godfrey, "Digital x-ray tomosynthesis: current state of the art and clinical potential", Physics in Medicine and Biology, 48, 2003.

[5] B.Wang, K.Barner, D.Lee, "Algebraic tomosynthesis reconstruction", Medical Imaging 2004, Proc. of SPIE Vol.5370.

[6] Y. Zhang, H-P.Chan, B. Sahiner, J. Wei, C. Zhou, L.M. Hadjiiski, "Artifact reduction methods for truncated projections in iterative breast tomosynthesis reconstruction", J. Comput. Assist. Tomogr.,33 n.3, 2009.

[7] K. Niinimäki, S. Siltanen, V. Kolehmainen, "Bayesian multiresolution method for local tomography in dental X-ray imaging", Physics in Medicine and Biology, 52, 6663-6678, 2007

[8] M. Bhatia, W.C. Karl, A.S. Willsky, "A wavelet-based method for multiscale tomographic reconstruction", IEEE Trans. on Medical Imaging, 15, 92-101, 1996.

[9] P. Chen, K.E. Barner, "Three-dimensional multi-resolution statistical reconstruction for tomosynthesis", Proc. of the IEEE Int. Symposium on Biomedical Imaging, 2004.